ELSEVIER

Journal of Non-Crystalline Solids 247 (1999) 58–63

JOURNAL OF NON-CRYSTALLINE SOLIDS

# Raman scattering, differential scanning calorimetry and $Nd^{3+}$ spectroscopy in alkali niobium tellurite glasses

Fabia C. Cassanjes [a,*], Younes Messaddeq [a], Luiz F.C. de Oliveira [b], Lilia C. Courrol [c], Laércio Gomes [c], Sidney J.L. Ribeiro [a]

[a] *Instituto de Química–UNESP, P.O. Box 355, Zip 14801-970, Araraquara, SP, Brazil*
[b] *Departamento Química, Universidade Federal de Juiz de Fora, Juiz de Fora, MG, Brazil*
[c] *Instituto de Pesquisas Energéticas e Nucleares–IPEN/CNEN, São Paulo, SP, Brazil*

**Abstract**

Alkali niobium tellurite glasses have been prepared and some of their properties measured by differential scanning calorimetry and Raman scattering. The vitreous domain was established in the pseudo ternary phases diagram for the system $TeO_2$–$Nb_2O_5$–($0.5K_2O$–$0.5Li_2O$). Raman scattering shows that for samples in the $TeO_2$ rich part of the phase diagram the vitreous structure is composed essentially of ($TeO_4$) units connected by the vertices, as in the α-$TeO_2$ crystal. The addition of alkali and niobium oxides causes depolymerization to occur with structures composed essentially of ($TeO_3$) and ($NbO_6$) units. Samples with the composition (mol%) $80TeO_2$–$10Nb_2O_5$–$5K_2O$–$5Li_2O$, stable against crystallization, were prepared containing up to 10% mol $Nd^{3+}$. The addition of this oxide increases the rigidity of the vitreous network shifting characteristic temperatures to higher temperatures. For the 10% $Nd^{3+}$ sample amorphous phase separation is assumed to exist from the observation of two glass transition temperatures. Spectroscopic properties such as Judd–Ofelt $\Omega_i$ intensity parameters, radiative emission probabilities, and induced emission cross sections were calculated. From these results and also from the emission quenching observed as a function of $Nd^{3+}$ concentration, we suggest that these glasses could be utilized in optical amplifying devices. 

## 1. Introduction

Tellurite glasses have scientific and technological interest due to their relatively higher refractive indices and dielectric constants and lower phonon energies compared for instance with the well known silicate or phosphate glasses. The refractive indices allow the utilization of these glasses for non-linear optical materials [1] and the phonon energies have at least two important consequences – improved infrared (IR) transmission (up to 6 μm) and low multiphonon decay rates for rare earths excited states as compared to silicate and phosphate glasses. Tellurite glasses are therefore potential candidates for IR transmitting devices and also hosts for IR emitting rare earths [2].

In a previous study we presented results on glass formation with the system $TeO_2$–$Nb_2O_5$–$Li_2O$–$K_2O$ [3]. A range of compositions may be obtained as stable glasses and in this work we present results on structural information obtained from Raman scattering spectra. Differential scanning calorimetry (DSC) data and the spectroscopic

* Corresponding author. Tel.: +55-16 232 2022; fax: +55-16 222 7932; e-mail: fabiacc@iq.unesp.br

0022-3093/99/$ – see front matter 
PII: S0022-3093(99)00074-5

characterization of $Nd^{3+}$ containing glasses are also presented.

## 2. Experimental

Appropriate mixtures of reagent-grade $TeO_2$ (3 N, aldrich) $Nb_2O_5$ (2 N, aldrich) $Li_2CO_3$ (mallinckrodt), $K_2CO_3$ (synth) were melted in gold crucibles for 30 min at 830°C in air. Liquids were quenched to room temperature in steel molds and annealing treatments were performed at temperatures near $T_g$ (glass transition temperature) for 30 min. Samples with composition (in mol%) $80TeO_2$–$10Nb_2O_5$–$5Li_2O$–$5K_2O$, stable against crystallization [3], were also prepared containing 0.5, 1.0, 2.0, 5.0 and 10% mol of $Nd^{3+}$ introduced in the starting batches in the form of the oxide.

Raman scattering spectra have been obtained from powdered samples with a microscopic raman spectrometer (Renishaw) with excitation from a He–Ne 30 mW laser (6345 Å). Differential scanning calorimetry scans (TA Instruments) were also obtained from powdered samples in closed aluminum pans at 10°C/min heating rate. Absorption spectra were obtained with 0.5 cm thick polished samples, in the visible and near infrared regions with a spectrophotometer (Cary-5). IR emission spectra were obtained with a spectrofluorimeter (Spex F121I) equipped with a 450 W Xe lamp as excitation source and a Ge detector (North Coast). Excited states lifetimes were obtained with 10 ns excitation pulses from a $N_2$ laser and a InSb detector. Emission signals were processed by a box car averager.

## 3. Results

Fig. 1 presents the vitreous domain obtained in the pseudo ternary phases diagram of the $TeO_2$–$Nb_2O_5$–($K_2O$–$Li_2O$) system [3]. Homogeneous samples with thickness $\leqslant 2$ cm could be obtained in the middle part of the vitreous domain. At the borders of this domain glassy samples were obtained by quenching liquids between two steel plaques. Table 1 and also the numbers in Fig. 1 identify the compositions studied here.

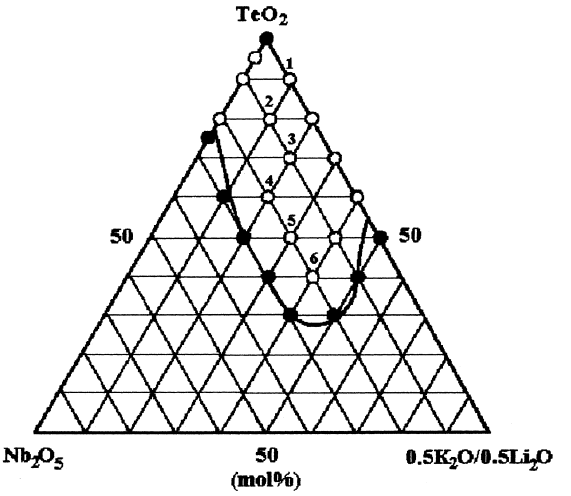


Fig. 1. Pseudo ternary phase diagram in the system $TeO_2$–$Nb_2O_5$–($0.5K_2O$–$0.5Li_2O$) showing the vitreous domain. Numbers denote compositions studied here. Open symbols – glasses, bold symbols – glass + crystals.

Fig. 2 shows Raman scattering spectra and here also the numbers identify the compositions for the sake of clarity. Starting from sample 1 a band is observed at 669 $cm^{-1}$ (band A) with a shoulder at around 765 $cm^{-1}$ (band B). A smaller amplitude band is observed at 472 $cm^{-1}$ (band C). On going from sample 1 to sample 6 an evolution is observed. Band C decreases and band B increases in amplitudes in comparison with the band A. In fact for sample 6 band B has the largest amplitude, centered at 765 $cm^{-1}$ and band A appears as a shoulder at around 670 $cm^{-1}$. Also another band is observed at 867 $cm^{-1}$ (band D) whose amplitude increases on going from sample 2 to 6. The $TeO_2$ spectrum also presented in Fig. 2 is dominated by two bands at 645 and 391 $cm^{-1}$. Smaller features are observed at 288, 337, 589, 718, 765 and 780 $cm^{-1}$. Maximum positions were measured with ±5 $cm^{-1}$ accuracy.

DSC results for these tellurite glasses have been discussed [3]. In Fig. 3 DSC scans obtained for the samples containing different concentrations of $Nd^{3+}$ are shown. The characteristic temperatures are presented in Table 1. With increase in the $Nd_2O_3$ content some general observations may be noted. There is an increase in $T_g$ values. Also the complex crystallization exotherm is shifted to

Table 1
Glass compositions (mol%) and characteristic temperatures (±1°C): $T_g$ (glass transition), $T_x$ (onset of glass crystallization), $T_c$ (maximum of the crystallization peak) and stability ($T_x-T_g$) parameter

| Sample | $TeO_2$ | $Nb_2O_5$ | ($0.5K_2O$–$0.5Li_2O$) | ($Nd^{3+}$) * | $T_g$ | $T_x$ | $T_c$ | ($T_x-T_g$) |
|---|---|---|---|---|---|---|---|---|
| 1 | 90 | – | 10 | – | 278 | 343 | 362 | 65 |
| 2 | 80 | 10 | 10 | – | 341 | 479 | 507 | 138 |
| 3 | 70 | 10 | 20 | – | 319 | 481 | 510 | 162 |
| 4 | 60 | 20 | 20 | – | 388 | 460 | 476 | 72 |
| 5 | 50 | 20 | 30 | – | 268 | 406 | 416 | 38 |
| 6 | 40 | 20 | 40 | – | 337 | 380 | 392 | 43 |
| 2–02 | 80 | 10 | 10 | 0.2 | 335 | 476 | 494 | 140 |
| 2–2 | 80 | 10 | 10 | 2 | 339 | 491 | 500 | 152 |
| 2–5 | 80 | 10 | 10 | 5 | 354 | 510 | 552 | 156 |
| 2–10 | 80 | 10 | 10 | 10 | 330–378 | 463 | 483–554 | – |

* $Nd^{3+}$ added to the base glass composition.

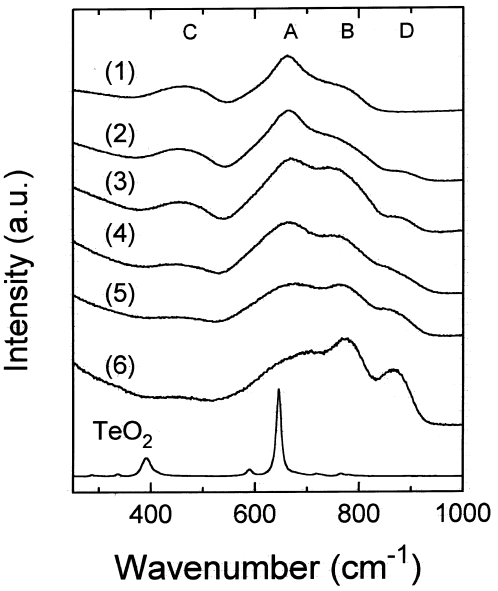


Fig. 2. Raman scattering spectra. Numbers identify the glass compositions.

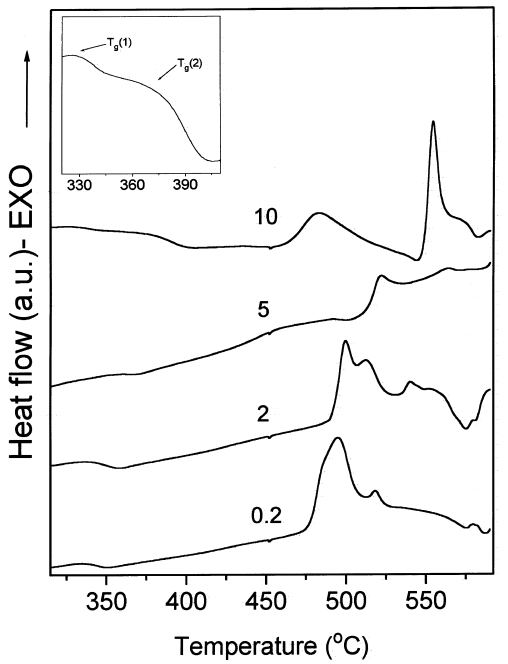


Fig. 3. DSC scans obtained for $Nd^{3+}$ containing glass with base composition (in mol%) $80TeO_2$–$10Nb_2O_5$–$10(0.5K_2O$–$0.5Li_2O)$. $Nd^{3+}$ content (mol%) is shown in the figure. Inset – Glass transition range for the 10% $Nd^{3+}$ sample.

higher temperatures from sample containing 0.2% $Nd^{3+}$ to the one containing 5% $Nd^{3+}$. The inset of Fig. 3 shows the $T_g$ region in detail for the sample containing 10% $Nd^{3+}$. Two $T_g$s may in fact be observed. Two well separated crystallization exotherms are also observed for this last sample. One at 483°C and a narrower one at 554°C.

Fig. 4(a) shows the absorption spectrum for the sample containing 1% mol $Nd^{3+}$ in which the electronic transitions between $^{2S+1}L_J$ levels of the $Nd^{3+}$ $4f^3$ configuration are detected. Assignments could be done by comparison with the literature [2] and intensities could be evaluated as usual from peak areas.

Electric dipole transition intensities were then calculated by Judd–Ofelt [4] analysis from experi-

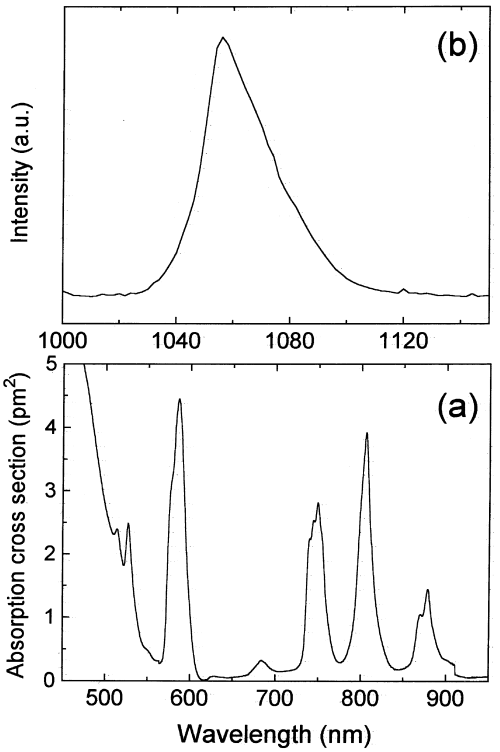


Fig. 4. (a) Absorption cross-section for 1% $Nd^{3+}$ sample; (b) $Nd^{3+}$ $^4F_{3/2} \rightarrow {}^4I_{11/2}$ emission spectrum.

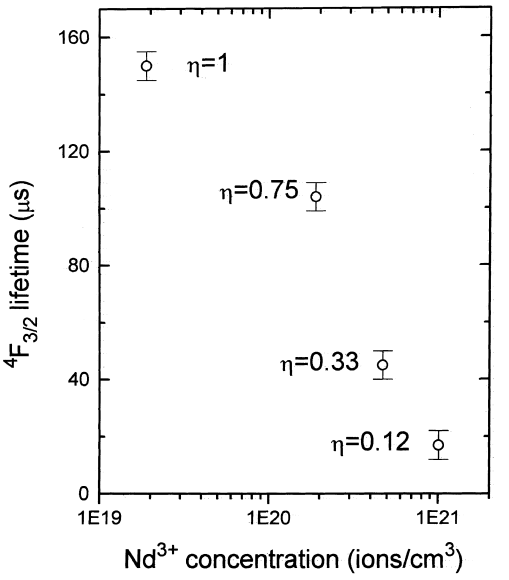


Fig. 5. $Nd^{3+}$ $^4F_{3/2}$ lifetime as a function of the $Nd^{3+}$ content. Quantum yields ($\eta = \tau_{EXP}/\tau_{RAD}$) are shown in the figure.

mental absorption data. $\Omega_\lambda$ ($\lambda = 2,4,6$) intensity parameters were obtained phenomenologically by a least squares fit of the measured absorption intensities. The $\Omega_\lambda$s obtained are (in units of $10^{-20}$ cm$^2$) $\Omega_2 = (3.9 \pm 0.4)$ $\Omega_4 = (4.8 \pm 0.5)$ and $\Omega_6 = (5.0 \pm 0.5)$. These $\Omega_\lambda$'s were used to obtain Einstein's spontaneous emission coefficient, $A = 7303$ s$^{-1}$, for the $Nd^{3+}$ $^4F_{3/2}$ excited state, where $A = \sum A_i$ and $A_i$ refer to all possible radiative transitions arising from $^4F_{3/2}$. Radiative lifetimes are given by the reciprocal of $A$ ($\tau_{rad} = 1/A$) and the lifetime $\tau_{RAD} = 134$ μs is compared with the experimental $\tau_{EXP} = (150 \pm 5)$ μs obtained for the sample containing 0.2% mol $Nd^{3+}$. The fluorescence branching ratios of the $^4F_{3/2}$ emitting level to the $^4I_{9/2}$, $^4I_{11/2}$, $^4I_{13/2}$ and $^4I_{15/2}$ levels were 0.44, 0.46, 0.095 and 0.005, respectively.

Fig. 4(b) displays the $Nd^{3+}$ $^4F_{3/2} \rightarrow {}^4I_{11/2}$ emission transition. The maximum ($\lambda_p$) is observed at 1056 nm and the effective bandwidth is 30.9 nm where $\Delta\lambda_{eff}$ is obtained by integration of the fluorescence line shape and dividing by the intensity at $\lambda_p$ [4].

Fig. 5 shows the evolution of the $^4F_{3/2}$ level lifetime as a function of the $Nd^{3+}$ concentration. Starting from the pure radiative lifetime obtained for the diluted sample, lifetimes are shortened and the decays become non-exponential with the increase in $Nd^{3+}$ concentration. In these cases lifetimes were calculated as the first 1/e folding time and $17 \pm 5$ μs is observed for the more concentrated sample. Fig. 5 also shows quantum efficiencies, taken as the ratio between the experimental and calculated lifetimes ($\eta = \tau_{EXP}/\tau_{RAD}$).

The induced peak emission cross section ($\sigma(\lambda_p)$) at 1056 nm was evaluated from its relationship with the spontaneous emission probabilities and bandwidths, given by the formula [4]:

$$\sigma_p(\lambda_p) = \frac{\lambda_p^4}{8\pi c n^2 \Delta\lambda_{eff}} A(^4F_{3/2} \rightarrow {}^4I_{11/2}), \quad (1)$$

where $n$ is the refractive index at $\lambda_p$. $\sigma(1056) = 4.1 \times 10^{-20}$ cm$^2$.

## 4. Discussions

### 4.1. Raman Spectra

α-$TeO_2$ belongs to the $D_4^4$ space group and the Raman bands are assigned following the work by Pine and Dresselhaus [5]. In this way the bands with the largest amplitudes at 391 and 645 $cm^{-1}$ are assigned to the $A_1$ vibrational mode. $B_1$, $B_2$, E(TO) and E(LO) modes are related to the smaller bands at 589, 780, 765 and 718 $cm^{-1}$, respectively. The structure of α-$TeO_2$ is built of ($TeO_4$) trigonal bipyramids connected at the vertices and the two bands at 391 and 645 $cm^{-1}$ have been assumed to be due to this structure. Spectra for samples 1 and 2 in the larger $TeO_2$ content part of the phases diagram in Fig. 1 are assumed to be an envelope of the crystalline $TeO_2$ spectrum. Therefore bands A and C are assigned to vibrations of ($TeO_4$) species. As we go further from the $TeO_2$ rich part in the vitreous domain these bands diminish in amplitude at the expense of an increase in amplitude of the component at 764 $cm^{-1}$. This last band is assigned to ($TeO_3$) trigonal pyramids and is due to the breakdown of the initially fully polymerized structure occurring with the addition of alkali and niobium oxide [6].

From sample 1 to sample 2 the addition of $Nb_2O_5$ is followed by the appearance of a new band, D, in the 860 $cm^{-1}$ region which is the same as that for Nb–O bonds in ($NbO_6$) groups [7]. On going from sample 4 to 6, the resolution of this band appears improved mainly due to the increase in amplitude of the tellurite band at 771 $cm^{-1}$.

### 4.2. DSC results

As already shown homogeneous and stable glasses are obtained in this system. The stability parameter $(T_x - T_g) = 138°C$ is obtained for the sample with composition (in mol%) $80TeO_2$–$10Nb_2O_5$–$5K_2O$–$5Li_2O$ [3].

With the addition of $Nd_2O_3$ important consequences in the stability of the glasses may be foreseen by observing DSC curves in Fig. 3. $T_g$ is shifted from 335 ± 1°C, to 354 ± 1°C on going from 0.2% to 5% $Nd^{3+}$ which we attribute to an increase in rigidity with the addition of this oxide. The crystallization exothermic peaks for these 3 samples, indicate a complex crystallization process. With increasing amounts of $Nd_2O_3$ the exothermic peaks are shifted to higher temperatures and change their shapes. $(T_x - T_g)$s also increase from 140 ± 1°C for the 0.2% Nd sample to 156 ± 1°C observed for the 5% Nd sample. Distinct features may be observed in the DSC scan obtained for the sample containing 10% mol $Nd^{3+}$. The inset of the Fig. 3 shows in detail the $T_g$ region for this sample. Two $T_g$s may be identified, labeled $T_g(1)$ at 330 ± 1°C and $T_g(2)$ at 378 ± 1°C. These two $T_g$s may be due to distinct amorphous phases in the glassy medium [8] despite the fact that the sample is macroscopically homogeneous and transparent. The two exotherms observed at 483 ± 1°C and 554 ± 1°C could well account for the crystallization of the two different glass phases but a more accurate study is needed to further explore this phenomenon.

### 4.3. $Nd^{3+}$ spectroscopy

The observed peak absorption cross sections in Fig. 3 are encouraging regarding potential applications as for mini lasers for example where such absorption is desirable for pumping efficiency. For example, the absorption cross section at the 806 nm region, for which pump diode lasers are available, is $4 \times 10^{-20}$ $cm^2$. This cross section is among the largest observed for glass samples [9]. The Judd–Ofelt $\Omega_\lambda$ intensity parameters and radiative probabilities compare well with those for other tellurite glasses [2]. The agreement between calculated and experimental lifetimes obtained for diluted samples indicates that the calculation of transition intensities is reliable. Also the quantum efficiency given by the ratio between these two lifetimes equals 1 (within experimental errors) due to negligible multiphonon contribution for the decay in these glasses.

Emission cross-sections are also the largest among oxide glasses [2], which we suggest indicates that these glasses could be utilized as rare earths containing amplifying devices. Recently laser action has been observed for bulk $Nd^{3+}$ containing tellurite glasses [10].

A quenching phenomenon due to ion–ion interaction is responsible for the decrease in lifetimes

observed with increase in $Nd^{3+}$ concentration [9]. Assuming that the decrease in lifetimes is due to this mechanism a quenching rate is defined as $R_Q = 1/\tau - 1/\tau_{rad}$ [9]. For the largest concentration ($1 \times 10^{21}$ ions $cm^{-3}$) here $R_Q = 4 \times 10^4$ which is intermediate between the $R_Q$s found for small quenching ($5 \times 10^3$ $s^{-1}$) and strong quenching ($5 \times 10^5$ $s^{-1}$) materials [11]. We suggest that these results for tellurite glass compositions show that they may be fabricated to optimize the compromise between the requeriment for absorption cross-section at the pump wavelength and the emission properties.

## 5. Conclusions

We propose that the Raman spectra of the alkali nioubium tellurite glasses in the $TeO_2$ rich compositions support the hypothesis that glass structures are fully polymerized network composed of ($TeO_4$) trigonal bipyramids is connected by the vertices as in a-$TeO_2$ crystalline phase. Increasing the concentration of alkali and niobium oxide ($TeO_3$) units are produced as a result of depolimerization processes.

The introduction of $Nd_2O_3$ increases the rigidity of the vitreous network. Based on the observation of two transition temperatures for the 10% mol $Nd^{3+}$ sample we conclude that there are two amorphous phases in this sample. Spectroscopic properties indicate that these glasses are potential hosts for light amplification devices.

## Acknowledgements

Authors acknowledge FAPESP, PRONEX, PADCT and CNPq (Brazilian agencies) for financial support, LEM (Laboratório de Espectroscopia Molecular), Instituto de Química, USP, São Paulo, for the utilization of the Raman spectrometer and LIEQ, UFSCAR, São Carlos) for the utilization of the spectrophotometer.

## References

[1] K. Shioya, T. Kmatsu, H.G. Kim, R. Sato, K. Matusita, J. Non-Cryst. Solids 189 (1995) 16.
[2] M.J. Waber, J.D. Meyers, D.H. Blackburn, J. Appl. Phys. 52 (4) (1981) 2944.
[3] F.C. Cassanjes, Y. Messaddeq, S.J.L. Ribeiro, Proceedings of the XVIII International Congress on Glass, July 5–10, 1998, San Francisco, CA, USA, C9, p. 101.
[4] W.F. Krupke, IEEE J. Quantum Electron. QE-10 (1974) 450.
[5] A.S. Pine, G. Dresselhaus, Phys. Rev. B 5 (10) (1972) 4087.
[6] A. Berthereau, E. Fargin, A. Villezusanne, R. Olazcuaga, G. Le Flem, L. Ducasse, J. Solid State Chem. 126 (1996) 143.
[7] A. El Jazouli, R. Brochu, J.C. Viala, R. Olazcuaga, C. Delmas, G. Le Flem, Ann. Chim. Fr. 7 (1982) 285.
[8] Z. Strnad, Glass–Ceramic Materials–Liquid Phase Separation, Nucleation and Crystallization in Glasses, in: Glass Science and Technology, vol. 8, Elsevier, Amsterdam, 1986, p. 145.
[9] R. Reisfeld, C.K. Jorgensen, Excited state phenomena in vitreous materials, in: K.A. Gschneidner, L. Eyring (Ed.), Handbook on the Physics and Chemistry of Rare Earths, Ch. 58, 1987, p. 1.
[10] N. Lei, B. Xu, Z. Jiang, Opt. Commun. 127 (1996) 263.
[11] F. Auzel, Mater. Res. Bull. 14 (1979) 223.